Mon. Not. R. Astron. Soc. **361,** 476–486 (2005) doi:10.1111/j.1365-2966.2005.09187.x

Time-dependent convection seismic study of δ Sct stars

M.-A. Dupret,[1,2]★ A. Grigahcène,[1] R. Garrido,[1] J. De Ridder,[4] R. Scuflaire[3] and M. Gabriel[3]

[1] *Instituto de Astrofísica de Andalucía-CSIC, Apartado 3004, 18080 Granada, Spain*
[2] *Observatoire de Paris, LESIA, 92195 Meudon, France*
[3] *Institut d'Astrophysique et de Géophysique de l'Université de Liège, Belgium*
[4] *Instituut voor Sterrenkunde, Katholieke Universiteit Leuven , Celestijnenlaan 200 B, 3001 Leuven, Belgium*

Accepted 2005 May 4. Received 2005 April 29; in original form 2005 January 10

ABSTRACT

We apply for the first time the time-dependent convection (TDC) treatment of Gabriel and Grigahcène et al. to the mode identification and seismic study of δ Sct stars. We consider the influence of this treatment on the photometric amplitude ratios and phase differences, and compare our TDC results to frozen convection (FC) results. We also compare the results obtained with different values of the mixing-length (ML) parameter α. Finally, we identify the modes and perform a seismic study of the stars V784 Cassiopeae (Cas), 1 Monocerotis (Mon) and 28 Andromedae (And), and show that our TDC models agree better with observations than FC models.

Key words: convection – stars: interiors – stars: oscillations – δ Scuti.

1 INTRODUCTION

δ Sct stars are variable A-F type stars located at the intersection region between the classical instability strip and the main sequence. Their pulsation periods ranges from 0.5 to 6 h and correspond to low order p and g, radial and non-radial modes. Many of these stars are multi-periodic, which makes them very good targets for asteroseismology. However, the mode identification (the first step of any seismic study) is particularly difficult for δ Sct stars. First, their frequency pattern is very complex because of the avoided crossings and the effect of rotation (often fast for these stars), so that mode identification based on their frequencies alone is impossible (contrary to solar-type oscillations). Secondly, photometric mode-identification techniques are very sensitive to the modelling of convection. Thirdly, the coupling of the modes due to rotation complicates both spectroscopic and photometric mode identifications, at least for fast rotators. In this paper, we consider the problem of convection, and we show that the use of time-dependent convection (TDC) models give theoretical amplitude ratios and phase lags in much better agreement with observations, which improves the reliability of photometric mode-identification methods for δ Sct stars.

Photometric observations of the amplitudes and phases in different colour passbands enable us to identify the degree ℓ of the modes. Two important theoretical ingredients in these methods are the amplitude (f_T) and phase (ψ_T) of local effective temperature variation for a normalized radial displacement. Garrido, Garcia-Lobo & Rodriguez (1990) and Garrido (2000) applied the method of Watson (1988) to δ Sct stars, considering f_T and ψ_T as free parameters. Still for δ Sct stars, Balona & Evers (1999) and Daszyńska-Daszkiewicz, Dziembowski & Pamyatnykh (2003) determined f_T and ψ_T using the non-adiabatic code of Dziembowski (1977) in which the diffusion approximation is assumed. Dupret et al. (2003a) and Moya, Garrido & Dupret (2004) included the improved perturbed atmosphere modelling of Dupret et al. (2002) in their computations. All these authors showed that for δ Sct stars, the non-adiabatic theoretical predictions are very sensitive to the value adopted for the mixing-length (ML) parameter α. The use of the convection theory of Canuto, Goldman & Mazzitelli (1996) has also been considered: Barban et al. (2003) computed new limb-darkening coefficients based on the atmosphere models by Heiter et al. (2002), and Dupret et al. (2004b) considered the inclusion of these new atmosphere models in their non-adiabatic computations. In all the above studies, a frozen convection (FC) approximation has been adopted. Dupret et al. (2004a, 2005) showed that, with the TDC treatment detailed in Grigahcène et al. (2005), it is possible to explain the location of the theoretical red edge of the δ Sct instability strip for radial and non-radial modes. For the first time, we present in this paper the application of TDC models to the study of the photometric amplitude ratios and phase differences in δ Sct stars.

2 INTERNAL STRUCTURE MODELS

The equilibrium stellar models have been computed by the evolutionary code CLÉS (Code Liégeois d'Évolution Stellaire). It uses the standard MLT for convection calculations, the OPAL opacities (Iglesias & Rogers 1996) completed at low temperatures with the opacities of Alexander & Ferguson (1994), the CEFF equation of state (Christensen-Dalsgaard & Däppen 1992) and the atmosphere models of Kurucz (1998) as boundary conditions. When not specified, the models of this study are computed with the global parameters $X = 0.7$, $Z = 0.02$ and convective core overshooting $\alpha_{\rm ov} = 0.2$.

★E-mail: MA.Dupret@obspm.fr

3 INFLUENCE OF TDC ON NON-ADIABATIC OBSERVABLES

In a linear one-layer approximation, the theoretical monochromatic magnitude variation of a non-radial mode is given by

$$\delta m_\lambda = -\frac{2.5}{\ln 10}\epsilon P_\ell^m(\cos i) b_{\ell\lambda}[-(\ell-1)(\ell+2)\,\cos(\sigma\,t) + f_T\,\cos(\sigma\,t+\psi_T)\,(\alpha_{T\lambda}+\beta_{T\lambda}) - f_g\,\cos(\sigma\,t)\,(\alpha_{g\lambda}+\beta_{g\lambda})]. \quad (1)$$

Some coefficients of equation (1) depend on the equilibrium atmosphere model: $b_{\ell\lambda} = \int_0^1 h_\lambda(\mu) P_\ell \,\mathrm{d}\,\mu$ (where $h_\lambda(\mu)$ is the normalized monochromatic limb-darkening law), $\alpha_{T\lambda} = \partial \ln F_\lambda / \partial \ln T_{\rm eff}|_g$, $\alpha_{g\lambda} = \partial \ln F_\lambda / \partial \ln g|_{T_{\rm eff}}$, $\beta_{T\lambda} = \partial \ln b_{\ell\lambda} / \partial \ln T_{\rm eff}|_g$, $\beta_{g\lambda} = \partial \ln b_{\ell\lambda} / \partial \ln g|_{T_{\rm eff}}$. Other coefficients: f_T and ψ_T (defined in Section 1) can only be obtained by non-adiabatic computations. f_g is the relative amplitude of effective gravity variation for a normalized radial displacement. Linear pulsation models do not give the absolute amplitudes. Theoretical amplitude ratios and phase differences between different photometric passbands can be determined by integrating equation (1) over the passbands and taking the complex ratios. This equation depends directly on the spherical degree ℓ of the modes. Therefore, confrontation between the theoretical and observed amplitude ratios and phase differences enables us to identify ℓ. Moreover, as f_T and ψ_T depend on the non-adiabatic pulsation models, comparison with observations enables us to constrain these models, a procedure we call non-adiabatic asteroseismology.

δ Sct stars at the blue side of the instability strip have two very thin superficial convective zones coinciding with the partial ionization zones of He II and H. Towards the red edge of the instability strip, these two thin convective zones merge into one single convective envelope (CE) whose size increases quickly as $T_{\rm eff}$ decreases. In non-adiabatic models, the coupling between the dynamical and thermal pulsation equations is taken into account. In particular, the perturbation of the radiative and convective flux must be determined in the CE. Most of the time, the perturbation of convection is neglected, which is the FC approximation.[1] However, this approximation is not justified for δ Sct stars because the lifetime of the convective elements is shorter than the pulsation periods in a significant part of their CE. The main goal of this paper is to present for the first time the theoretical photometric amplitude ratios and phase differences obtained with TDC models and to compare them with FC models.

For the results obtained with TDC treatment presented in this section, only the perturbation of convective flux is taken into account. Similar results are obtained when the perturbations of turbulent pressure and dissipation rate of turbulent kinetic energy are also taken into account. We begin by giving in Fig. 1 the evolution from ZAMS to TAMS of f_T and ψ_T as function of $T_{\rm eff}$, for the fundamental radial mode and models with $M = 1.8$ M$_\odot$, $Z = 0.02$ and different values of α. We compare the results obtained with TDC and FC models. Main differences occur for ψ_T. At the blue side of the instability strip ($T_{\rm eff} \gtrsim 8000$ K), the different models give similar results. But as $T_{\rm eff}$ decreases, the size of the CE increases so that different convection models give very different ψ_T. Typical observed values of ψ_T for δ Sct stars are between 90° and 140°, which agree with our TDC theoretical predictions. In contrast, the low values of ψ_T encountered for the cold FC models with large α are unrealistic. Models with masses and metallicities different from the ones of Fig. 1 give similar results for a given $T_{\rm eff}$ and α.

[1] Different FC approximations exist (Pesnell 1990). The case considered in this paper is to ignore the Lagrangian variations of convective luminosity, turbulent pressure and dissipation rate of turbulent kinetic energy.

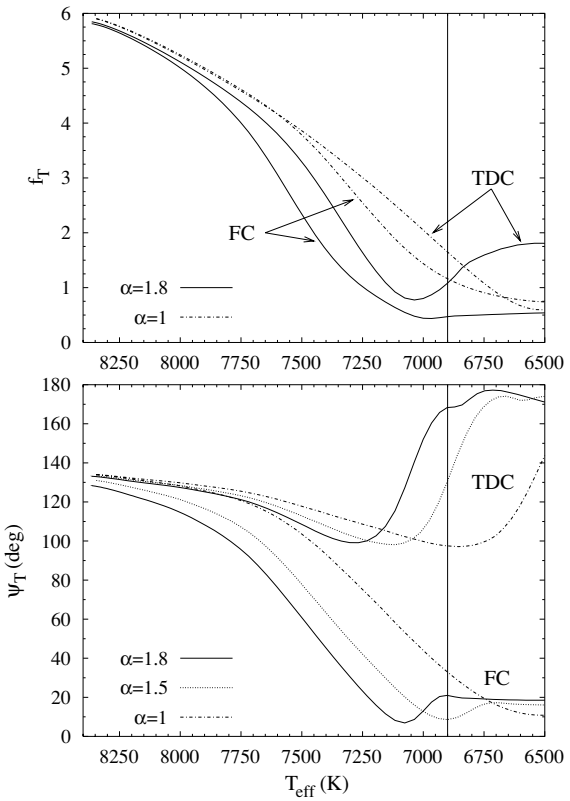

Figure 1. Evolution of the normalized amplitude of the effective temperature variation f_T (top panel) and the phase lag ψ_T (bottom panel) as a function of $T_{\rm eff}$, for the fundamental radial mode, obtained with TDC and FC non-adiabatic models with $M = 1.8$ M$_\odot$ and different α. The vertical line gives the location of the observational red edge of the δ Sct instability strip.

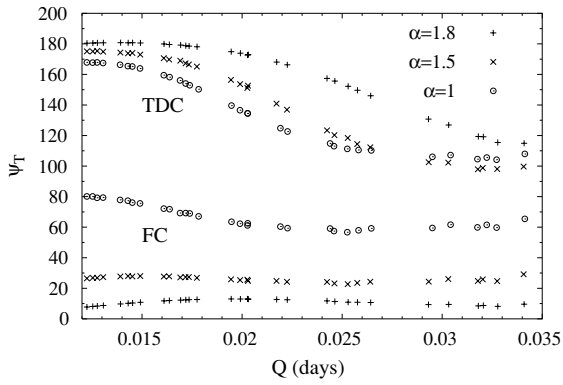

Figure 2. Phase lag ψ_T as a function of the constant of pulsation Q, obtained with TDC and FC models with $M = 1.8$ M$_\odot$, $T_{\rm eff} = 7120$ K and different α.

For a given model, f_T and ψ_T are also dependent on the pulsation frequency. In Fig. 2, we give the values of ψ_T as function of the constant of pulsation $Q = P\sqrt{(\mathrm{R}_\odot/R)^3(M/\mathrm{M}_\odot)}$ (P is the period in days, for the fundamental radial mode $Q \simeq 0.033$ d, $\tau_{\rm dyn}/\tau_{\rm dyn,\odot} = \sqrt{(R/\mathrm{R}_\odot)^3(\mathrm{M}_\odot/M)} = 3.104282$ for this model). We compare the results obtained with TDC and FC non-adiabatic models and modes with $0 \leqslant \ell \leqslant 3$ and $m = 0$. Equilibrium models have

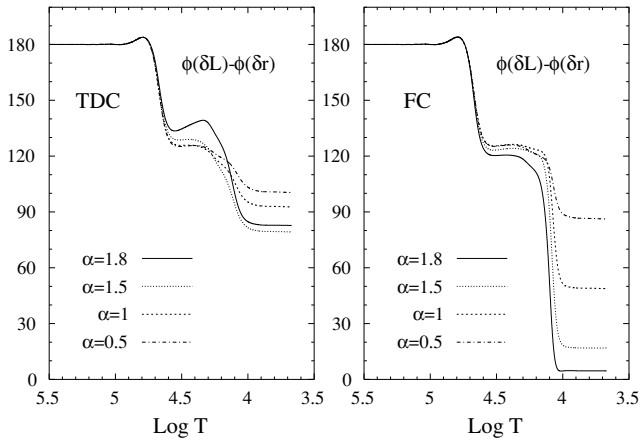

Figure 3. Phase difference between the total luminosity variation and the radial displacement (in degrees) as a function of $\log T$, for the fundamental radial mode, obtained with TDC models (left) and FC models (right) with $M = 1.8$ M$_\odot$, $T_{\rm eff} = 7120$ K and different α.

$M = 1.8$ M$_\odot$, $T_{\rm eff} = 7120$ K, $Z = 0.02$ and different values of α. All the modes given in Fig. 2 are predicted to be unstable. Again, we see a significant difference between the TDC and FC phase lags. This difference increases with α, simply because the size of the CE, and thus the sensitivity to the convection treatment, increases with α. The phase lag depends heavily on the period in the TDC case. $\psi_T \simeq 100^\circ$ near the fundamental radial period, then it increases as the period decreases, up to values around the adiabatic 180° when the stable region ($Q \leqslant 0.0125$ for the $\alpha = 1.8$ model) is reached.

In order to understand the origin of the difference between the TDC and FC phase lags, we give in Fig. 3 the phase difference between the total luminosity variation and the radial displacement ($\phi(\delta L) - \phi(\delta r)$) (in degrees) as a function of $\log T$, for the fundamental radial mode and the same models as in Fig. 2. The left panel gives TDC results and the right panel gives FC results. In the deep regions ($\log T > 5$), the pulsation is quasi-adiabatic with a phase lag of 180°. Then, the first phase lag quasi-independent of the convection treatment occurs in the partial ionization zone of He II ($4.9 \geqslant \log T \geqslant 4.6$). Finally, a phase lag appears in the partial ionization zone of H ($4.2 \geqslant \log T \geqslant 4$). The latter is very large for cold FC models with large α, which leads to phase lags close to 0° at the surface, while on the contrary, it is much smaller for TDC models. We also see that the TDC phase lags are less sensitive to α than the FC ones. The occurrence of the phase lags can be interpreted as follows. In δ Sct models, $\phi(\delta r)$ is quasi-constant (except around the nodes) and most of the phase lag comes from variations of $\phi(\delta L)$. Using the equation of energy conservation and $\phi(\delta L) = \Im(\ln(\delta L))$, we have for a radial mode:

$$\Delta\phi(\delta L) = \int \frac{{\rm d}\phi(\delta L)}{{\rm d}m}{\rm d}m = \int \Im\left\{\frac{{\rm d}\delta L/{\rm d}m}{\delta L}\right\}{\rm d}m$$
$$= -\int \Re\left\{\frac{\sigma T \delta s}{\delta L}\right\}{\rm d}m \cong -\int \Re\left\{\frac{\delta s/c_{\rm v}}{\delta L/L}\right\}\frac{c_{\rm v} T\sigma}{L}{\rm d}m. \quad (2)$$

From this equation, we see that significant phase lag can occur if the thermal relaxation time is significant compared to the pulsation period (case of the He II partial ionization zone) and/or the pulsation is highly non-adiabatic (case of the H partial ionization zone). The sensitivity of the FC results to α can be understood as follows (see also Moya et al. 2004). In the FC approximation, $\Re\{\delta s L/(c_{\rm v}\delta L)\}$ is large in the convective zone coinciding with the H partial ionization zone (HCZ), therefore large phase lags occur in this zone, according to equation (2). When α increases, the mass of the HCZ increases quickly. As there is an integration over the mass in equation (2), the phase lag appearing in this zone increases with α. The large values of $|\delta s/c_{\rm v}|$ occurring in the HCZ and FC case are not allowed by TDC models because they would lead to large superadiabatic gradients and thus too large variations of the convective flux. Therefore, the phase lags in the HCZ are smaller in the TDC case than in the FC case. As α increases, convection becomes more efficient and TDC models force $|\delta s/c_{\rm v}|$ to be even smaller in this zone; this counterbalances the increase of the HCZ mass with α, so that the TDC phase lags are less sensitive to α than the FC ones. The phase lag occurring in the partial ionization zone of He II is not sensitive to α because the fraction of energy transported by convection is negligible in this zone. The return of the phase lags to 180° in TDC models towards the red edge of the instability strip (see Fig. 1) is more difficult to interpret. It is associated with positive values of d $\phi(\delta L)$/d m in the intermediate region between the He II and H partial ionization zones ($4.6 \geqslant \log T \geqslant 4.3$), which can be seen in the left panel of Fig. 3 (solid line, $\alpha = 1.8$).

According to equation (1) and using the values of f_T and ψ_T computed by our non-adiabatic pulsation code, we can determine the amplitude ratios and phase differences of magnitude variation in different photometric passbands. Classical diagrams used for photometric mode identification with the Strömgren photometry (Garrido et al. 1990) represent in abscissa the phase difference $\phi(b-y) - \phi(y)$ and in ordinate the amplitude ratio $A(b-y)/A(y)$. Such a diagram is represented in Fig. 4. The curves give the values of these quantities along the evolution sequence of stellar models with $M = 1.8$ M$_\odot$, $Z = 0.02$, $\alpha = 1.5$ and effective temperatures from 8200 K (•) down to 7100 K (○). Solid lines are for TDC models and dotted lines for FC models. Results are given for modes of degrees $\ell = 0$, 1 and 2; for each ℓ, we selected the mode with frequency closest to the one of the fundamental radial mode. As expected, there is no significant difference between TDC and FC results for hot models. On the contrary, for cold models at the red side of the instability strip, the differences are significant in view of typical observational error bars (a fraction to a few degrees for the phases and a few per cent for the amplitudes).

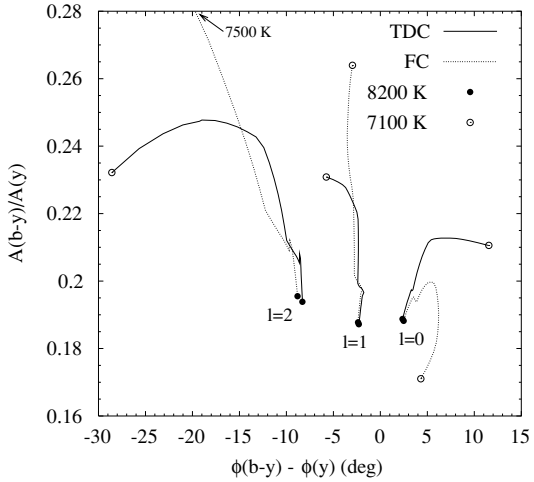

Figure 4. The evolution of the phase difference $[\phi(b-y) - \phi(y)]$ and the amplitude ratio $[A(b-y)/A(y)]$ for the Strömgren photometry, $\ell = 0$, 1, 2 modes, TDC and FC treatments and equilibrium models with $T_{\rm eff}$ between 8200 K (•) and 7100 K (○).

4 APPLICATIONS

We now consider the applications to different specific δ Sct stars. The main goal of this paper is to confront the predictions of our non-adiabatic models to the observed amplitude ratios and phase differences. Moreover, we have shown in Section 3 that the main difference between FC and TDC theoretical results is in the phase lag ψ_T for models at the red side of the instability strip. Therefore, we chose to study the δ Sct stars for which the most precise multi-colour photometric amplitudes and phases are available, for which (if possible) simultaneous spectroscopic and photometric observations were performed (giving the phase difference between the light and velocity curves) and located at the red side of the instability strip. As the modelling of the rotation–pulsation interaction and the influence of rotation on the equilibrium models remains subject to uncertainties and is not taken into account in our study, we selected stars with small or moderate $v \sin i$. We do not study stars with too many frequencies, for which the estimate of the amplitudes and phases could be biased by unresolved modes. Also, we do not consider monoperiodic high-amplitude δ Sct stars for which the light curve is strongly non-linear, because our pulsation modelling is linear.

The methodology of our non-adiabatic seismic study is the following. First, we identify the degree ℓ of the modes by confronting the theoretical and observed amplitude ratios and phase differences for some models. Secondly, we compute a large grid of models with different M, $T_{\rm eff}$, α and Z inside the global parameters observational error box. If one of the modes is identified as radial, we only consider models fitting exactly the frequency of this mode (considering it either as the fundamental or as the first overtone). Then, we perform non-adiabatic computations with TDC and FC treatments for all these models and determine the theoretical amplitude ratios and phase differences between different photometric passbands. For the stars with simultaneous spectroscopic and photometric observations, we also determine the theoretical phase lag between the velocity and the light curves. For the confrontation with multi-colour photometric observations, we use the following discrimant:

$$\chi^2 = \frac{1}{2N} \sum_{\substack{i=1 \\ i \neq i_0}}^{N+1} \left[\frac{\left(A_i^{\rm t}/A_{i_0}^{\rm t} - A_i^{\rm o}/A_{i_0}^{\rm o} \right)^2}{\sigma_{{\rm a}i}^2} + \frac{\left(\Delta\phi_i^{\rm t} - \Delta\phi_i^{\rm o} \right)^2}{\sigma_{\phi i}^2} \right], \quad (3)$$

where $N+1$ is the number of filters, $A_i^{\rm t}$ and $A_i^{\rm o}$ are the theoretical and observed amplitudes in the filter i, i_0 is the reference filter, $\Delta\phi_i^{\rm t}$ and $\Delta\phi_i^{\rm o}$ are the theoretical and observed phase differences between the filters i and i_0, and $\sigma_{{\rm a}i}$ and $\sigma_{\phi i}$ are the standard errors for the observed amplitude ratios and phase differences. Comparing the discriminants obtained for different models enables us to determine which convection models agree best with observations. The seismic study presented in this paper is concentrated on the fitting of the amplitude ratios and phase differences more than on the fitting of the frequencies; frequency fitting including the effect of rotation will be considered in future works.

In the applications, we adopt the following conventions for the different non-adiabatic treatments of the convection–pulsation interaction: TDC1 stands for time-dependent convection models including only the perturbation of convective flux; TDC2 stands for time-dependent convection models including the perturbation of convective flux, turbulent pressure and dissipation rate of turbulent kinetic energy into heat and FC stands for Frozen Convection models. The way the different terms of our TDC treatment are determined is detailed in Grigahcène et al. (2005).

For the determination of the monochromatic flux derivatives and limb-darkening coefficients required in equation (1), we consider the results obtained with two different families of atmosphere models. On the one hand, we use the atmosphere models of Kurucz (1993) and the limb-darkening coefficients of Claret (2000), in which the ML treatment of convection ($\alpha = 1.25$) is adopted, we refer to them as MLT atmosphere models. On the other hand, we use the new atmosphere models of Heiter et al. (2002) and the limb-darkening coefficients of Barban et al. (2003), in which the convection treatment of Canuto et al. (1996) is adopted, we refer to them as FST atmosphere models.

4.1 V784 Cassiopeae

The variability of V784 Cassiopeae (Cas) (HD 13122) was discovered by the *Hipparcos* satellite. This star was observed in the Johnson and Strömgren *vby* photometry and in medium-resolution spectroscopy between 1999 and 2001 by Kiss et al. (2002). They detected four frequencies: $f_1 = 9.1565$ c/d, $f_2 = 9.4649$ c/d, $f_3 = 15.4036$ c/d and $f_4 = 15.9013$ c/d.

4.1.1 Global parameters and equilibrium models

There is no Hβ measure for V784 Cas and the dereddening could not be estimated. Therefore, the photometric determinations of the effective temperature and gravity must be considered with caution. For the metallicity, Gray, Napier & Winklet (2001) noted that it is a mild Am star, the lines of Sr II λ4077 and λ4216 are enhanced. There is no abundance determination in the literature. The observed global parameters obtained with different calibrations are given in Table 1.

In Table 2, we give the global characteristics of some of the equilibrium models we considered for V784 Cas. As will be confirmed

Table 1. Observed global parameters of V784 Cas.

$T_{\rm eff}$ (K)	$\log (L/{\rm L}_\odot)$	$\log g$	[M/H] (km s^{-1})	$v \sin i$
6980[a]	1.3(0.06)[e]	3.86[a]	0.38[d]	55(10)[e]
6990[b]		3.73[b]	0.53[b]	66(10)[f]
7100(100)[c]		3.8(0.1)[c]		

Strömgren indices-based calibrations are taken from [a]Smalley & Kupka (1997), [b]Stütz & Nendwich (2002), [c]Kurucz (1998) and [d]Smalley (1993). [e]Luminosity is deduced from the *Hipparcos* parallax (Kiss et al. 2002). [e]$v \sin i$ determinations are taken from [e]Kiss et al. (2002) and [f]De Medeiros & Mayor (1999). Error bars are given in parentheses.

Table 2. Global parameters of some of the theoretical models adopted for V784 Cas. Models 1–8 fit f_1 as the fundamental radial mode and models 9–12 fit f_1 as the first overtone.

Model	$M/{\rm M}_\odot$	$T_{\rm eff}$ (K)	$\log (L/{\rm L}_\odot)$	$\log g$	Z	α
1	1.80	6966	1.1931	3.8250	0.02	1.8
2	1.80	6976	1.1927	3.8280	0.02	1.5
3	1.80	6984	1.1924	3.8304	0.02	1.0
4	1.80	6959	1.1930	3.8234	0.02	0.5
5	2.20	6998	1.2521	3.8610	0.05	1.8
6	2.20	7014	1.2512	3.8659	0.05	1.5
7	2.25	7155	1.2921	3.8695	0.05	1.8
8	2.25	7148	1.2925	3.8673	0.05	1.5
9	1.95	6898	1.3473	3.6886	0.02	1.8
10	1.95	6915	1.3474	3.6928	0.02	1.5
11	1.95	6920	1.3473	3.6941	0.02	1.0
12	1.95	6910	1.3474	3.6914	0.02	0.5

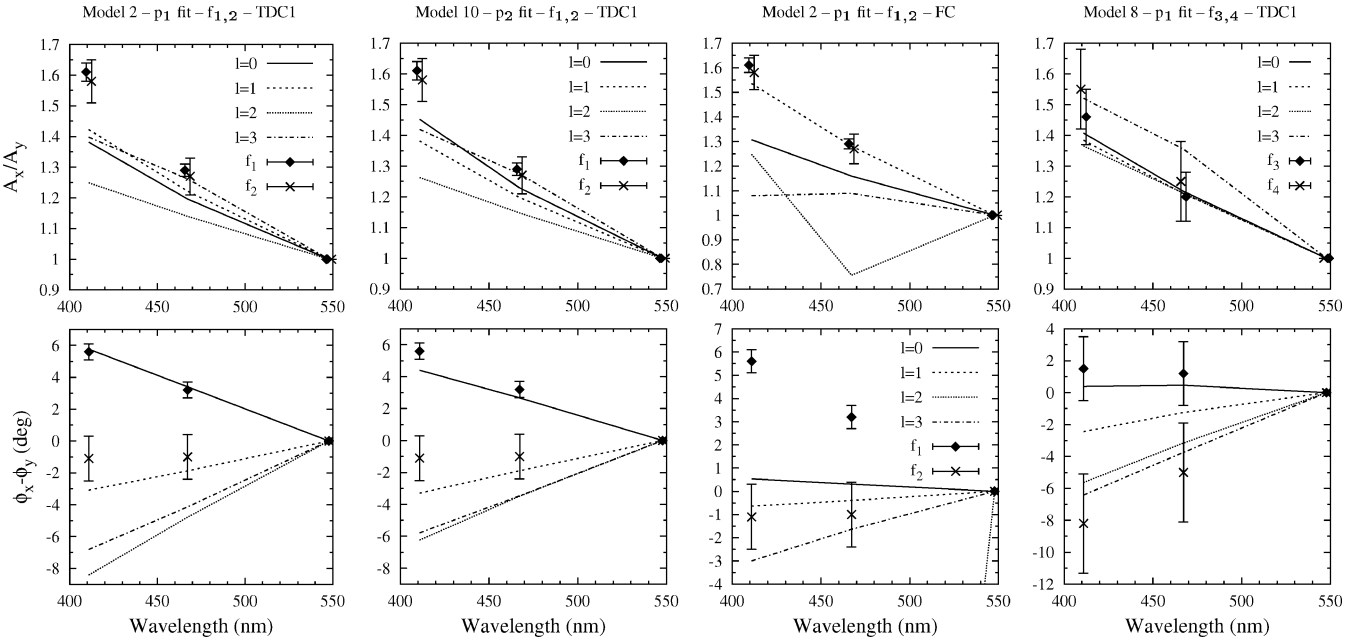

Figure 5. Amplitude ratios (top panels) and phase differences (bottom panels) for different models of V784 Cas. The lines are the theoretical predictions for different ℓ, and the error bars represent the observations for f_1 and f_2 (six left panels) and for f_3 and f_4 (two right panels).

in this study, the main frequency $f_1 = 9.1565$ c/d is clearly identified as a radial mode. However, because of the global parameter uncertainties, it is not clear if it is the fundamental mode or the first overtone. For each evolutionary sequence considered in our study, we selected the model fitting f_1 exactly as the fundamental radial mode and the colder model fitting f_1 exactly as the first radial overtone, which gives two families of models. In Table 2, models 1–8 fit f_1 as the p_1 radial mode and models 9–12 fit f_1 as the p_2 mode. All the models of Table 2 are with $X = 0.7$ and core overshooting $\alpha_{ov} = 0.2$. We considered models with different values of the ML parameter α: 0.5, 1, 1.5 and 1.8 with $Z = 0.02$ and with a high metallicity ($Z = 0.05$) suggested by the photometric calibrations.

4.1.2 Mode identification

Depending on the models and non-adiabatic treatments (TDC or FC), different theoretical amplitude ratios and phase differences are obtained. All these models identify without any doubt f_1 as a radial mode and f_2 as an $\ell = 1$ mode. This mode identification does not depend on the initial choice of the model and is therefore reliable. As an illustration of this mode identification, we give in Fig. 5 (four left panels) the confrontation between the theoretical and observed amplitude ratios (top panels) and phase differences (bottom panels), as obtained with our TDC1 treatment, for two different models fitting f_1 as the p_1 mode (left) or the p_2 mode (right). For all the models of Fig. 5, we used FST atmospheres. For f_3 and f_4, the observational error bars are larger. We did not find a model fitting at the same time the amplitude ratios and phase differences for the four modes of V784 Cas. In the two right panels of Fig. 5, we give the comparison between the theoretical amplitude ratios and the phase differences for the TDC1 model 8 and the observations for f_3 and f_4. We see that f_3 is identified most likely as a radial mode, while f_4 could be an $\ell = 2$ or an $\ell = 3$ mode. In Table 3, we give a summary of the mode identification. Given the uncertainties on the global parameters of V784 Cas, it is not possible to know whether f_1 is the fundamental or the first overtone. Confrontation with the observed amplitudes and phases does not help to discriminate between these two possibilities, as shown by the four left panels of Fig. 5. The row 'p_1 fit' ('p_2 fit') of Table 3 gives the radial orders of the different modes if f_1 is considered as the fundamental radial mode (the first overtone).

Table 3. Mode identification for the four frequencies of V784 Cas.

	f_1	f_2	f_3	f_4
ℓ	$\ell = 0$	$\ell = 1$	$\ell = 0$	$\ell = 2$ or 3
p_1 fit	p_1	g_1	p_3	p_1 or f
p_2 fit	p_2	p_1	p_5	p_3 or p_1

4.1.3 Results obtained with different convection models

We now compare the results obtained with different convection models. In Table 4, we give the discriminants (square roots of equation 3) obtained for the four frequencies of V784 Cas. In columns 2–5, we give the index of the model in Table 2, the mass, the mixing-length parameter and the metallicity. In column 6, we give the radial order of the mode fitting f_1. In column 7, we give the treatment of convection in the atmosphere. In column 8, we give the adopted treatment of convection–pulsation interaction in the interior. $\chi_{1,0}$ is the discriminant for f_1, considering it as a radial mode; $\chi_{2,1}$ is the discriminant for f_2, considering it as an $\ell = 1$ mode; $\chi_{3,0}$ is the discriminant for f_3, considering it as a radial mode; $\chi_{4,2}$ is the discriminant for f_4, considering it as an $\ell = 2$ mode and $\chi_{4,3}$ is the discriminant for f_4, considering it as an $\ell = 3$ mode.

As the error bars for the f_1 frequency are by far the lowest, the models with smallest values of $\chi_{1,0}$ can be considered as the models giving the best agreement with observations. Rows 1–4 of Table 4 give the best models obtained using FST atmospheres. All these best models were obtained with TDC treatment. Rows 5–8 give the results obtained for the same models but with MLT atmospheres. For V784 Cas, the results obtained with the two types of atmosphere models are not very different. We note that solar metallicity is used in all the FST atmospheres, while the MLT atmosphere of model 5 (row 7) is with [M/H] = 0.5, which agrees better with observations.

Table 4. Discriminants obtained for different models and for the four frequencies of V784 Cas. Explanation is given in Section 4.1.3

Model		$M/M_\odot$	α	Z	n_{f_1}	conv.		$\chi_{1,0}$	$\chi_{2,1}$	$\chi_{3,0}$	$\chi_{4,2}$	$\chi_{4,3}$
1	10	1.95	1.5	0.02	p_2	FST	TDC2	3.245	1.949	0.581	1.725	1.577
2	10	1.95	1.5	0.02	p_2	FST	TDC1	3.315	1.758	0.586	1.633	1.531
3	5	2.20	1.8	0.05	p_1	FST	TDC1	3.414	1.435	0.475	1.661	1.530
4	1	1.80	1.8	0.02	p_1	FST	TDC1	3.574	1.649	0.524	1.734	1.648
5	10	1.95	1.5	0.02	p_2	MLT	TDC2	4.172	1.463	0.513	1.695	1.603
6	10	1.95	1.5	0.02	p_2	MLT	TDC1	2.819	1.363	0.509	1.624	1.573
7	5	2.20	1.8	0.05	p_1	MLT	TDC1	3.029	1.084	0.595	1.583	1.534
8	1	1.80	1.8	0.02	p_1	MLT	TDC1	5.275	1.405	0.572	1.715	1.663
9	2	1.80	1.5	0.02	p_1	FST	TDC1	4.482	1.424	0.430	1.674	1.404
10	3	1.80	1.0	0.02	p_1	FST	TDC1	5.053	1.070	0.314	1.242	0.809
11	4	1.80	0.5	0.02	p_1	FST	TDC1	5.110	1.088	0.367	1.271	0.997
12	2	1.80	1.5	0.02	p_1	FST	TDC2	5.158	1.578	0.448	1.741	1.417
13	3	1.80	1.0	0.02	p_1	FST	TDC2	5.071	1.057	0.267	1.229	0.758
14	4	1.80	0.5	0.02	p_1	FST	TDC2	5.124	1.079	0.350	1.223	0.910
15	6	2.20	1.5	0.05	p_1	MLT	TDC1	3.820	0.696	0.513	1.108	0.904
16	7	2.25	1.8	0.05	p_1	MLT	TDC1	4.293	0.815	0.465	1.068	0.821
17	8	2.25	1.5	0.05	p_1	MLT	TDC1	4.957	0.801	0.443	0.729	0.431
18	9	1.95	1.8	0.02	p_2	FST	TDC1	5.064	1.623	0.545	1.658	1.747
19	11	1.95	1.0	0.02	p_2	FST	TDC1	5.340	1.203	0.634	1.432	1.210
20	12	1.95	0.5	0.02	p_2	FST	TDC1	5.605	1.135	0.592	1.473	1.413
21	2	1.80	1.5	0.02	p_1	FST	FC	8.376	0.427	0.579	3.871	11.051
22	3	1.80	1.0	0.02	p_1	FST	FC	6.810	0.716	0.491	2.091	5.120
23	4	1.80	0.5	0.02	p_1	FST	FC	5.586	0.981	0.326	0.605	0.583
24	10	1.95	1.5	0.02	p_2	FST	FC	7.695	0.255	0.586	2.060	16.488
25	11	1.95	1.0	0.02	p_2	FST	FC	6.838	0.552	0.759	1.422	6.123
26	12	1.95	0.5	0.02	p_2	FST	FC	5.905	0.979	0.789	0.777	0.494

Rows 4–9 to 11 give the 1.8 $M_\odot$ TDC1 results obtained with different values of the mixing length parameter α. As shown in Section 3, the TDC results are not very sensitive to α, the best ones correspond to $\alpha = 1.8$ (solar calibrated value). Rows 12–14 give the results for the same models but with the TDC2 treatment. Comparison with rows 9–11 shows that the inclusion of the turbulent pressure and dissipation rate of turbulent kinetic energy perturbations does not significantly change the results. Rows 7 and 15–17 give the results obtained with $Z = 0.05$ (as suggested by the photometric calibration). We see that the results are less sensitive to the metallicity than to α and $T_{\rm eff}$. Rows 2 and 18–20 give the results obtained fitting f_1 as the p_2 radial mode (instead of p_1). The confrontation with the observed amplitudes and phases does not allow to determine whether f_1 is the p_1 or the p_2 radial mode. Rows 21–26 give the results obtained with FC treatment. For f_1, we see that the discriminants are much larger with FC treatment than with TDC treatment. This shows that TDC results agree better with observations than FC ones (see also Fig. 5). As shown in Section 3, TDC and FC results are the closest for small α. For the $\ell = 1$ mode (f_2), the agreement with observations is better for FC models, but the observational error bars are much larger for this mode and TDC results remain in relatively good agreement with observations. We note that V784 Cas was observed simultaneously in photometry and spectroscopy (Kiss et al. 2002). However, there are not enough radial velocity measurements to determine the amplitudes and phases of each individual mode. A simple look at fig. 7 of Kiss et al. (2002) shows that the light and velocity curves are approximately in opposite phase, in agreement with our TDC results. Finally, we remark that no constraints can be deduced from the mode excitation. For all the models we have considered, all the modes are predicted to be unstable in the range of observed frequencies.

4.1.4 f_1/f_3 *frequency ratio*

The frequencies f_1 and f_3 of V784 Cas are identified as radial modes. We compared the theoretical ratios of radial modes with different n to the observed ratio $f_1/f_3 = 0.594439$, for many models with metallicities $0.02 \leqslant Z \leqslant 0.05$, hydrogen mass fraction $0.65 \leqslant X \leqslant 0.75$ and core overshooting parameter $0 \leqslant \alpha_{\rm ov} \leqslant 0.25$. The models fitting f_1 as the fundamental radial mode and f_3 as the second overtone give $0.6166 \leqslant f_{p_1}/f_{p_3} \leqslant 0.620$. The lowest frequency ratios are obtained for models with high X and Z. The models fitting f_1 as the first overtone and f_3 as the fourth overtone give $0.569 \leqslant f_{p_2}/f_{p_5} \leqslant 0.5706$. We see that the theoretical frequency ratios are poorly sensitive to the global parameters of the model and none of the theoretical results agree with the observed frequency ratio (0.5944). Suarez (2002) and Suarez et al. (in preparation) show that the frequency ratios of radial modes predicted by models taking the effect of rotation into account are different from the case without rotation. Helium diffusion was discussed as another possible explanation for unusual (high) first overtone to fundamental period ratios (Cox, McNamara & Ryan 1984; Guzik & Cox 1991). In future works we will analyse whether rotation and/or diffusion is able to explain the observed frequency ratios of V784 Cas.

4.2 1 Monocerotis

1 Monocerotis (Mon) (HD 40535) is a δ Sct star with three clearly observed frequencies: $f_1 = 7.346146$ c/d, $f_2 = 7.475268$ c/d and $f_3 = 7.217139$ c/d (Balona & Stobie 1980). Balona et al. (2001) observed this star simultaneously in the Strömgren *uvby* and Cousins *I* photometry and in high-dispersion spectroscopy, which is of particular interest for our study. They identified f_1 as a radial mode and f_2 as most likely $(\ell_2, m_2) = (1, -1)$.

Table 5. Observed global parameters of 1 Mon.

$T_{\rm eff}$ (K)	$\log (L/L_\odot)$	$\log g$	[M/H]	$v \sin i$ (km s^{-1})
7240[a]	1.45(0.07)[g]	3.77[a]	0.2[d]	18.8(1.5)[h]
7113[b]		3.47[b]	0.19[b]	
7080[c]				
7100(100)[e]				
$\geqslant$ 6885[f]				

Strömgren indices-based calibrations are taken from [a]Smalley & Kupka (1997), [b]Stütz & Nendwich (2002), [c]Moon & Dworetsky (1985) and [d]Smalley (1993). [e]Profile fitting based on the Hβ line and [f]the Hα line is taken from Solano & Fernley (1997). [g]The luminosity is deduced from the *Hipparcos* parallax (Balona et al. 2001). [h]$v \sin i$ determination is taken from Solano & Fernley (1997).

Table 6. Global parameters of some of the theoretical models considered for 1 Mon. Models 1–7 fit f_1 as the fundamental radial mode and models 8–10 fit f_1 as the first overtone.

	$M/M_\odot$	$T_{\rm eff}$ (K)	$\log (L/L_\odot)$	$\log g$	α
1	1.95	6981	1.3466	3.7101	1.5
2	1.95	6988	1.3465	3.7120	1.0
3	1.95	7002	1.3463	3.7156	0.5
4	2.05	7281	1.4377	3.7137	1.8
5	2.05	7293	1.4374	3.7169	1.5
6	2.05	7288	1.4375	3.7157	1.0
7	2.05	7282	1.4376	3.7142	0.5
8	2.10	6888	1.4884	3.5771	1.5
9	2.10	6875	1.4886	3.5736	1.0
10	2.10	6860	1.4888	3.5698	0.5

4.2.1 Global parameters and equilibrium models

The observed global parameters of 1 Mon obtained with different calibrations are given in Table 5. There is no abundance determination for this star. In Table 6, we give the global characteristics of some of the equilibrium models we considered for 1 Mon. As we will confirm in this study, the main frequency $f_1 = 7.346146$ c/d is clearly identified as a radial mode. However, because of the global parameter uncertainties, it is not clear if it is the fundamental mode or the first overtone. For each evolutionary sequence considered in our study, we selected the model fitting exactly f_1 as the fundamental radial mode and the colder model fitting exactly f_1 as the first radial overtone, which gives two families of models: in Table 6, models 1–7 fit f_1 as the p_1 radial mode and models 8–10 fit f_1 as the p_2 mode. All the models of Table 6 have $X = 0.7$, $Z = 0.02$ and core overshooting $\alpha_{\rm ov} = 0.2$. We considered models with different values of the ML parameter α: 0.5, 1, 1.5 and 1.8.

4.2.2 Mode identification

For 1 Mon, observations in the Strömgren *uvby* and Cousins *I* (infrared) passbands are available along with simultaneous observations in high-dispersion spectroscopy. This enables to identify the modes with a higher degree of confidence. From the observations of Balona et al. (2001), only the two frequencies $f_1 = 7.346146$ c/d and $f_2 = 7.475268$ c/d have sufficiently precise amplitudes and phases for mode identification, and we consider only these two frequencies in our study. Depending on the models and non-adiabatic treatments (TDC or FC), different theoretical amplitude ratios and phase differences are obtained. In our study of 1 Mon, we have used the atmosphere models of Kurucz (1993) for the determination of the quantities $\alpha_{T\lambda}$, $\alpha_{g\lambda}$, ... of equation (1). All our models (TDC and FC) identify f_1 as a radial mode and f_2 as an $\ell = 1$ mode. As an illustration of this mode identification, we give in Fig. 6 the confrontation between the theoretical and observed photometric amplitude ratios (top panels), photometric phase differences (middle panels) and phase differences between magnitude variation and radial displacement (bottom panels), for different models of 1 Mon. The six left panels give the results obtained with TDC treatment including the perturbation of convective flux and the six right panels give the results obtained with FC treatment. Index of the models is given at the top of the panels, according to Table 6. As said before, it is not clear if f_1 is the fundamental mode or the first overtone, we consider thus the two cases. We see that the confrontation with the observed phases gives a slightly better agreement for model 10 (p_2 fit) than for model 5 (p_1 fit), but in view of the error bars, we do not consider this as enough to discriminate between these two possibilities. We note that our models are not able to give a good agreement with the observed phase in the *u* filter. Photometric mode identification based on TDC models is better than with FC; however in the case of 1 Mon it appears that both TDC and FC give the same in pure photometry (see top and middle panels of Fig. 6). Balona et al. (2001) also did a photometric mode identification of f_1 and f_2, using the non-adiabatic code of Dziembowski (1977), which does not include TDC. They also performed a spectroscopic mode identification (based on the line profile variations). Both mode identifications of Balona et al. (2001) are compatible with ours.

4.2.3 Results obtained with different convection models

We now compare the results obtained with different convection models. As 1 Mon has been observed simultaneously in multi-colour photometry and in spectroscopy, we can define different discriminants for the confrontation between theory and observations. First, we use the photometric discriminant defined by the square root of equation (3). For this discriminant, we use the *y* filter as reference (as in Fig. 6) because the amplitudes and phases are subject to more theoretical uncertainties at smaller wavelengths. Secondly, we use another discriminant for the confrontation between the theoretical and observed phase differences between the magnitude variations and the radial velocity curve. This discriminant is defined as follows:

$$\chi^2_V = \frac{1}{N+1} \sum_{i=1}^{N+1} \left[\frac{\left(\Delta\phi^{\rm t}_{i,V} - \Delta\phi^{\rm o}_{i,V} \right)^2}{\sigma^2_{\phi i,V}} \right], \qquad (4)$$

where $N+1$ is the number of filters, $\Delta\phi^{\rm t}_{i,V}$ and $\Delta\phi^{\rm o}_{i,V}$ are the theoretical and observed phase differences between the magnitude variation in filter i and the radial velocity variation and $\sigma_{\phi i,V}$ are the standard errors for the observed phase differences. χ_V gives the best discrimination between the different convection models, because $\Delta\phi^{\rm t}_{i,V}$ is closely related to the phase lag ψ_T, which is very sensitive to the convection treatment (see Fig. 1).

In Table 7, we give the values obtained for these discriminants for different models. In column 2, we give the index of the model whose global parameters are given in Table 6. In column 3, we give the adopted treatment of convection–pulsation interaction. Then, we give the different discriminants. $\chi_{V1,0}$ is the magnitude–velocity discriminant (equation 4) for f_1, considering it as a radial mode; $\chi_{V2,1}$ is the magnitude–velocity discriminant for f_2, considering it as an $\ell = 1$ mode; $\chi_{1,0}$ is the photometric discriminant (equation 3)

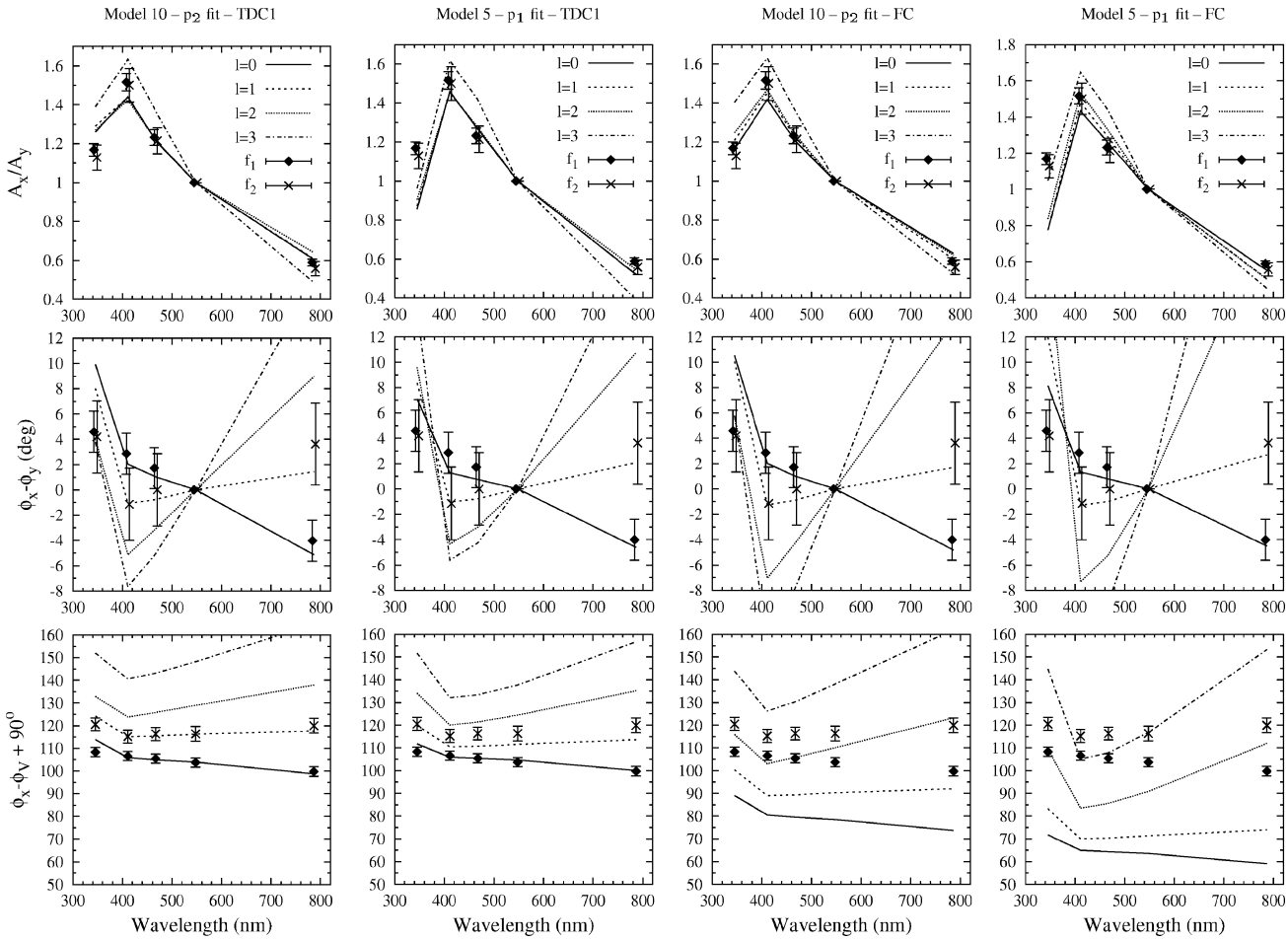

Figure 6. Photometric amplitude ratios $A_{u,v,b,y,I}/A_y$ (top panels), photometric phase differences $\phi_{u,v,b,y,I} - \phi_y$ (middle panels) and phase differences between magnitude variation and radial displacement $\phi_{u,v,b,y,I} - \phi_{V_r} + 90^\circ$ (bottom panels), for different models of 1 Mon. The lines are the theoretical predictions for different ℓ and the error bars represent the observations for f_1 and f_2.

Table 7. Discriminants obtained for different models and for the two main frequencies of 1 Mon. Explanation is given in Section 4.2.3.

Model		Conv.	$\chi_{V1,0}$	$\chi_{V2,1}$	$\chi_{1,0}$	$\chi_{2,1}$
1	10	TDC1	1.229	0.681	1.712	1.166
2	10	TDC2	1.707	1.156	1.726	1.160
3	3	TDC1	1.799	2.111	1.987	0.702
4	5	TDC1	0.798	1.586	3.834	1.581
5	8	TDC1	6.661	1.731	3.997	2.047
6	9	TDC1	4.456	2.439	2.034	1.264
7	8	TDC2	9.333	2.225	5.213	2.417
8	9	TDC2	7.670	3.920	2.352	1.388
9	1	TDC1	12.640	6.683	2.724	0.956
10	2	TDC1	6.389	4.779	1.937	0.687
11	4	TDC1	2.627	3.137	3.925	1.666
12	6	TDC1	3.256	0.657	3.774	1.518
13	7	TDC1	4.920	1.494	3.744	1.482
14	8	FC	44.176	32.657	4.601	2.262
15	9	FC	32.779	23.554	3.162	1.349
16	10	FC	11.934	8.499	1.767	0.989
17	1	FC	43.643	31.936	4.579	2.177
18	2	FC	29.507	21.072	3.091	1.322
19	3	FC	9.061	7.075	2.167	0.834
20	5	FC	19.395	14.632	4.507	2.249
21	6	FC	5.893	5.766	4.011	1.759
22	7	FC	3.539	0.731	3.777	1.516

for f_1, considering it as a radial mode; and $\chi_{2,1}$ is the photometric discriminant for f_2, considering it as an $\ell = 1$ mode. Rows 1–4 of Table 7 give the models that agree best with observations. All these models were obtained with TDC treatment. Some are with small α (models 10 and 3, $\alpha = 0.5$), others with larger α (model 5, $\alpha = 1.5$). Model 10 fits f_1 as the first radial overtone while models 3 and 5 fit f_1 as the fundamental radial mode. Therefore, present observations do not allow to discriminate between these possibilities. Rows 1, 5 and 6 give the 2.1 $M_\odot$, p_2 fit results obtained with different values of the mixing length parameter α, taking the perturbation of convective flux into account (TDC1). Rows 2, 7 and 8 give the results for the same models, but taking also the perturbation of turbulent pressure and dissipation rate of turbulent kinetic energy into account (TDC2). Rows 3, 9 and 10 give the 1.95 $M_\odot$, p_1 fit results obtained with different α and TDC1 treatment. For the 1.95 and 2.1 $M_\odot$ models, the best agreement is found with $\alpha = 0.5$. Rows 4, 11, 12 and 13 give the 2.05 $M_\odot$, p_1 fit results obtained with different α and TDC1 treatment. We see that for this mass, the best agreement is obtained with $\alpha = 1.5$. Rows 14–22 give the results obtained for the same models but with FC treatment. In the case of 1 Mon, considering only the photometric amplitudes and phases does not allow to reject the small α FC results compared to the TDC results. But for the magnitude–velocity phase lags, the TDC results agree much better with observations than the FC ones, as shown by the discriminants $\chi_{V1,0}$ and $\chi_{V2,1}$ and the bottom panels of Fig. 6. In agreement with

the general discussion in Section 3, TDC and FC results are the closest for small α.

4.2.4 Other possible constraints

No constraint can be deduced from the mode excitation. For all the models we have considered, all the modes are predicted to be unstable in the range of observed frequencies.

For the comparison between the theoretical and observed frequencies, the present observations are not sufficient to give more constraints on the models. In our study, we have already used the information given by f_1: all our selected models fit f_1 exactly, either as the fundamental radial mode or as the first overtone. Concerning f_2, it is identified as an $\ell = 1$ mode and the spectroscopic mode identification of Balona et al. (2001) indicates that its azimuthal order is $m = -1$. As the other components of the triplet are not observed and the inclination angle is not known with sufficient precision, we can not yet use this frequency to constrain the model.

4.3 28 Andromedae

28 Andromedae (And) (HD 2628) is a δ Sct star known to show extreme amplitude changes. It has a main pulsation frequency $f_1 = 14.4292$ c/d. Rodriguez et al. (1993) obtained precise Strömgren photometric amplitudes and phases, and 5 years later, Rodriguez et al. (1998) found the amplitude to be 19 times less. Rodriguez et al. (1998) also revealed the existence of a secondary frequency $f_2 = 17.23$ c/d.

4.3.1 Global parameters and equilibrium models

The observed global parameters of 28 And obtained from photometry and spectroscopy are given in Table 8. In Table 9, we give the global characteristics of some of the theoretical models we considered for 28 And. As we will show in this study, the main frequency $f_1 = 14.4292$ c/d is a non-radial mode. As its azimuthal order m is unknown, trying to fit this frequency would be useless. We therefore computed several equilibrium models in the observational error box, without frequency based constraint, as given in Table 9. All these models have $X = 0.7$, $Z = 0.02$ and core overshooting $\alpha_{\rm ov} = 0.2$. We considered models with different values of the ML parameter α: 0.5, 1, 1.5 and 1.8.

4.3.2 Mode identification

In this section and in Section 4.3.3, we consider the multi-colour photometric amplitudes and phases given by Rodriguez et al. (1993) for the confrontation with observations. We computed the theoretical amplitude ratios and phase differences for all the models given in Table 9 and it clearly appears that the main mode of 28 And is non-radial, which is somehow unusual for mono-periodic δ Sct stars. Confrontation with observations shows that it is probably an $\ell = 2$ mode, which could be p_1 or p_2 depending on the model. As an illustration of this mode identification, we give in the four left panels of Fig. 7, the TDC amplitude ratios and phase differences obtained for two models with $\alpha = 1.5$ and $\alpha = 1$. The $\alpha = 1.5$ model is in very good agreement with observations. The right panels of Fig. 7 show that the FC amplitudes and phases do not agree with observations. For all the models of Fig. 7, we used FST atmospheres.

Table 8. Observed global parameters of 28 And.

$T_{\rm eff}$ (K)	$\log g$	[M/H]	$v \sin i$ (km s^{-1})
7240[a]	3.72[a]	−0.13[c]	16.1(1.5)[g]
7249[b]	3.67[b]	−0.13[b]	
7300[d]	3.85[d]	−0.16(0.24)[f]	
7350[e]	3.65[e]		

Strömgren indices-based calibrations are taken from: [a]Smalley & Kupka (1997), [b]Stütz & Nendwich (2002) and [c]Smalley (1993). [d]Hγ profile fitting using MLT and [e]Canuto & Mazzitelli convection models are taken from Adelman et al. (2000). [f]Detailed abundances determination was performed by Adelman et al. (2000). [g]$v \sin i$ determination is taken from Solano & Fernley (1997).

Table 9. Global parameters of the 28 And theoretical models.

Model	$M/{\rm M}_\odot$	$T_{\rm eff}$ (K)	$\log (L/{\rm L}_\odot)$	$\log g$	α
1	2.1	7308	1.4835	3.6850	1.8
2	2.1	7287	1.4838	3.6797	1.5
3	2.1	7282	1.4839	3.6782	1.0
4	2.1	7274	1.4840	3.6764	0.5
5	2.0	7371	1.3881	3.7739	1.5
6	2.0	7251	1.3907	3.7428	1.5
7	2.0	7234	1.3910	3.7385	1.0
8	2.0	7219	1.3913	3.7347	0.5

4.3.3 Results obtained with different convection models

In Table 10, we give the discriminants (square roots of equation 3) obtained for different ℓ. In column 2, we give the index of the model whose global parameters are given in Table 9. In column 3, we give the convection treatment in the atmosphere model. In column 4, we give the adopted treatment of convection–pulsation interaction. Then, we give the discriminants, first for $\ell = 2$ which gives the best agreement with observations, and then for other ℓ (0, 1 and 3). Rows 1–4 of Table 10 give the best models obtained using FST atmospheres. All these best models were obtained with TDC treatment. Rows 5–8 give the results obtained for the same models but with MLT atmospheres. Rows 9–14 give the TDC1 results obtained for 2.0 and 2.1 ${\rm M}_\odot$ models with different values of the mixing length parameter α. As shown in Section 3, the TDC results are not very sensitive to α, for 28 And the best agreement with observations is found with $\alpha = 1.5$. Rows 15–18 give the results obtained with FC treatment. Comparing the TDC and FC results shows that TDC results agree more closely with observations than FC ones. TDC and FC results are the closest for small α. Finally, we remark that no constraints can be deduced from the mode excitation. For all the models we have considered, all the modes are predicted to be unstable in the range of observed frequencies.

4.3.4 Amplitudes and phase changes between the 1991 and 1996 seasons

The amplitudes of 28 And diminished by a factor of 19 between 1991 and 1996, without any significant frequency change (Rodriguez et al. 1993, 1998). We compared the photometric amplitude ratios and phase differences of the two seasons and give them in Fig. 8. In the same figure, we also give the theoretical results for our best model (model 2, TDC1 treatment of convection). There is a significant difference in the observed amplitude ratios and phase differences between the two seasons; these changes cannot be explained by our models – we cannot be completely sure that we are seeing the same mode, but there is no clear indication that we are seeing a different

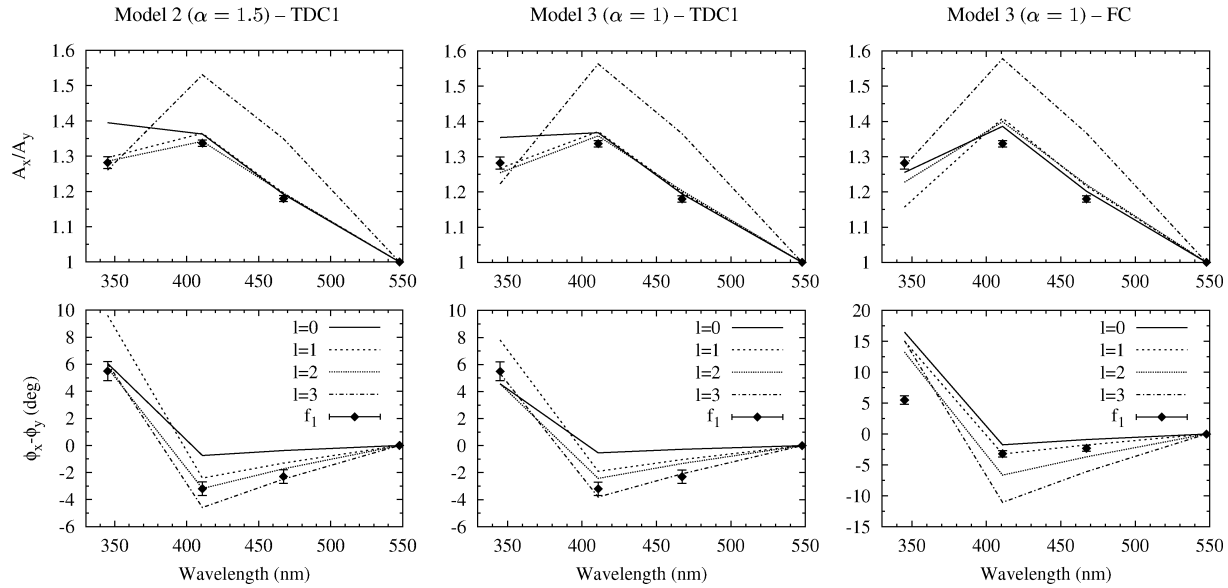

Figure 7. Amplitude ratios (top panels) and phase differences (bottom panels) for different models of 28 And (the four left panels are for TDC models and the two right panels are for FC models). The lines are the theoretical predictions for different ℓ, and the error bars represent the observations (1991 season).

Table 10. Discriminants for different ℓ and models of 28 And. Explanation is given in Section 4.3.3.

Model		conv.		$\chi_{\ell=2}$	$\chi_{\ell=0}$	$\chi_{\ell=1}$	$\chi_{\ell=3}$
1	2	FST	TDC1	0.870	3.951	3.003	11.745
2	1	FST	TDC1	1.096	5.701	3.268	10.213
3	3	FST	TDC2	1.209	3.786	2.991	12.492
4	2	FST	TDC2	1.222	5.039	3.610	10.516
5	2	MLT	TDC1	1.344	4.211	3.297	8.177
6	1	MLT	TDC1	1.958	6.175	3.721	7.536
7	3	MLT	TDC2	1.209	4.028	3.175	8.510
8	2	MLT	TDC2	2.106	5.391	3.998	7.789
9	3	FST	TDC1	1.963	3.634	2.691	13.358
10	4	FST	TDC1	2.470	3.931	2.624	13.993
11	5	FST	TDC1	4.311	6.314	5.063	13.419
12	6	FST	TDC1	2.907	5.450	2.947	11.055
13	7	FST	TDC1	3.134	4.430	2.493	13.293
14	8	FST	TDC1	2.978	4.081	2.576	14.028
15	1	FST	FC	27.562	15.082	18.600	38.469
16	2	FST	FC	18.883	15.615	14.825	28.448
17	3	FST	FC	6.540	7.083	7.312	16.541
18	4	FST	FC	2.111	3.554	2.906	13.938

one. Amplitude changes are often interpreted as the effect of non-linear coupling with another mode with close frequency. It would be interesting to examine in future work if such coupling can explain the case of 28 And.

5 CONCLUSIONS

Mode identification is a key step in any asteroseismic study. In this paper, we have presented the details of the significant improvement obtained by using TDC non-adiabatic models for the photometric mode identification in δ Sct stars. The treatment of convection plays a major role in the theoretical determination of the photometric amplitude ratios and phase differences. Therefore, comparison with observations enables us to constrain the convection treatment adopted in the equilibrium models as well as the treatment of the non-

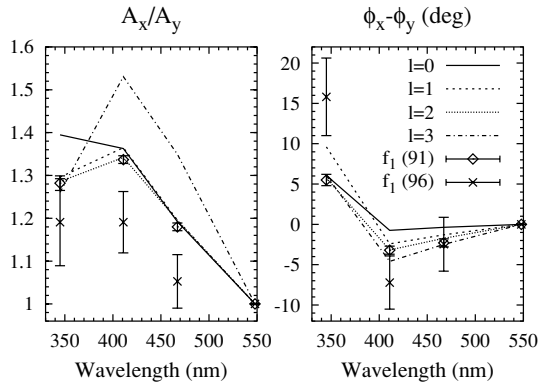

Figure 8. Amplitude ratios (left panel) and phase differences (right panel), as observed in 1991 ($\diamond$) and in 1996 ($\times$). The lines are the theoretical predictions for different ℓ and for model 2 (TDC).

adiabatic interaction between convection and pulsation, a method we call non-adiabatic asteroseismology. We applied this method to the three stars V784 Cas, 1 Mon and 28 And.

For V784 Cas, we identified the four modes as $\ell_1 = 0$, $\ell_2 = 1$, $\ell_3 = 0$ and $\ell_4 = 2$ or 3. The best agreement between the theoretical and observed photometric amplitude ratios and phase differences was obtained for TDC models with $\alpha \simeq 1.8$ (solar calibrated value). FC results do not agree with observations. Theoretical results with high metallicity agree slightly better with observations than those with solar metallicity. It is not yet possible to determine whether the main frequency is the fundamental radial mode or the first overtone. Also, it is not yet possible to obtain an agreement between the theoretical and observed frequency ratios f_1/f_3.

For 1 Mon, we identified the two main modes as $\ell_1 = 0$ and $\ell_2 = 1$, confirming the results of Balona et al. (2001). Main differences between TDC and FC results appear in the phase lag between the photometric magnitude variations and the velocity curve; the best agreement between theory and observation was obtained for TDC models with different α. The light-velocity phase lags given by FC models do not agree with observations. In agreement with Balona et al.

(2001), we confirm that multi-colour photometry with longer wavelength coverage (here by including Cousins I passband observations), as well as simultaneous photometric and spectroscopic observations significantly improve the mode identification. It is not yet possible to determine if the main frequency of 1 Mon is the fundamental radial mode or the first overtone.

For 28 And, we identified the main mode as an $\ell = 2$ mode. Very good agreement between the theoretical and observed photometric amplitude ratios and phase differences was obtained for TDC models with $\alpha \simeq 1.5$. FC results disagree with observations. The huge amplitude change between 1991 and 1996 cannot be explained by the present theory.

For these three stars, the largest differences between different convection treatments appear in the phase differences, and TDC results agree better with observations than FC results. Also, the phase differences give more discrimination than the amplitude ratios for the mode identification. It is thus very important to use TDC models for the photometric mode identification and seismic study of δ Sct stars, at least for cold ones with $T_{\rm eff} \lesssim 7500$ K. However, our TDC models do not succeed yet in matching at the same time all frequencies, amplitudes and phase differences. Different reasons could explain this. The coupling of the modes due to rotation could affect the amplitude ratios and phase differences and is not included in our models. The effects of rotation and diffusion are not taken into account in our equilibrium models. We are also aware that some uncertainties are still associated with our TDC treatment and that it could be improved, for example, by considering non-local and anisotropic aspects of turbulence and theories more sophisticated than MLT. We will consider this in our future works. In this paper, we presented the mode identification and seismic study of three specific stars. A complete study of many other δ Sct stars will be presented in future works. Also, we will present a more detailed comparison between the results obtained with MLT and FST atmospheres in our future works.

ACKNOWLEDGMENTS

MAD acknowledges financial support from CNES. AG and RG acknowledge financial support from the program ESP2001-4528-PE. JDR acknowledges support from the Fund for Scientific Research-Flanders.

REFERENCES

Adelman S. J., Caliskan H., Kocer D., Cay I. H., Gokmen T. H., 2000, MNRAS, 316, 514
Alexander D. R., Ferguson J. W., 1994, ApJ, 437, 879
Balona L. A., Evers E. A., 1999, MNRAS, 302, 349
Balona L. A., Stobie R. S., 1980, MNRAS, 190, 931
Balona L. A. et al., 2001, MNRAS, 321, 239
Barban C., Goupil M. J., Van't Veer-Menneret C., Garrido R., Kupka F., Heiter U., 2003, A&A, 405, 1095
Canuto V. M., Goldman I., Mazzitelli I., 1996, ApJ, 473, 550
Christensen-Dalsgaard J., Däppen W., 1992, A&A, Rev., 4, 267
Claret A., 2000, A&A, 363, 1081
Cox A. N., McNamara B. J., Ryan W., 1984, ApJ, 284, 250
Daszyńska-Daszkiewicz J., Dziembowski W. A., Pamyatnykh A. A., 2003, A&A, 407, 999
De Medeiros J. R., Mayor M., 1999, A&AS, 139, 433
Dupret M.-A., De Ridder J., Neuforge C., Aerts C., Scuflaire R., 2002, A&A, 385, 563
Dupret M.-A. et al., 2003a, Ap&SS, 284, 129
Dupret M.-A., De Ridder J., De Cat P., Aerts C., Scuflaire R., Noels A., Thoul A., 2003b, A&A, 398, 677
Dupret M.-A., Grigahcène A., Garrido R., Gabriel M., Scuflaire R., 2004a, A&A, 414, L17
Dupret M.-A., Grigahceňe A., Garrido R., Montalban J., Gabriel M., Scuflaire R., 2004b, in Kurtz D. W., Pollard K., eds, ASP Conf. Ser. Vol. 310, Variable Stars in the Local Group. Astron. Soc. Pac., San Francisco, p. 470
Dupret M.-A., Grigahcène A., Garrido R., Gabriel M., Scuflaire R., 2005, A&A, 435, 927
Dziembowski W., 1977, Acta Astron., 27, 95
Gabriel M., 1996, Bull. Astron. Soc. India, 24, 233
Garrido R., 2000, in Montgommery M., Breger M., eds, The 6th Vienna Workshop on δ Scuti and Related Stars, PASP Conf. Ser., 210, 67
Garrido R., Garcia-Lobo E., Rodriguez E., 1990, A&A, 234, 262
Gray R. O., Napier M. G., Winklet L. I., 2001, AJ, 121, 2148
Grigahcène A., Dupret M.-A., Gabriel M., Garrido R., Scuflaire R., 2005, A&A, 434, 1055
Guzik J. A., Cox A. N., 1991, Delta Scuti Newsletter, Issue 3
Heiter U. et al., 2002, A&A, 392, 619
Iglesias C. A., Rogers F. J., 1996, ApJ, 464, 943
Kiss L. L., Derekas A., Alfaro E. J., Biro I. B., Csak B., Garrido R., Szatmary K., Thomson J. R., 2002, A&A, 394, 97
Kurucz R. L., 1993, ATLAS9 Stellar Atmosphere Programs and 2 km s^{-1} Grids, Kurucz CDROM No 13
Kurucz R. L., 1998, http://kurucz.harvard.edu/grids.html
Moon T. T., Dworetsky M. M., 1985, MNRAS, 217, 305
Moya A., Garrido R., Dupret M.-A., 2004, A&A, 414, 1081
Pesnell W. D., 1990, ApJ, 363, 227
Rodriguez E., Rolland A., Lopez de Coca P., Garrido R., Mendoza E. E., 1993, A&A, 273, 473
Rodriguez E., Rolland A., Lopez-Gonzalez M. J., Costa V., 1998, A&A, 338, 905
Smalley B., 1993, A&A, 274, 391
Smalley B., Kupka F., 1997, A&A, 328, 349
Solano E., Fernley J., 1997, A&AS, 122, 131
Stütz C., Nendwich J., 2002, Vienna TempLogG v2 web interface: http://ams.astro.univie.ac.at/templogg/main.php References for the calibrations in the manual at http://ams.astro.univie.ac.at/templogg/Manual.php
Suarez J. C., 2002, PhD thesis
Watson R. D., 1988, Ap&SS, 140, 255

This paper has been typeset from a TEX/LATEX file prepared by the author.